Electronic Supplementary Material (ESI) for Journal of Materials Chemistry A.

Supporting Information

Triphenylamine-contained dihydrophenazine copolymers with adjustable multi-electron redox characteristics and its application as cathode for lithium-organic batteries

Lihuan Xu,[a] Qiang Fei [a] and Chang Su[a*]

[a] College of Chemical Engineering, Shenyang University of Chemical Technology, Shenyang, 110142, P. R. China.

*Corresponding author. Tel.: +86-24-89383902; Fax: +24-89383902.

E-mail address: suchang@syuct.edu.cn (Chang Su);

Table of Contents

11. Supplementary for equivalent circuit data of p-DTPAPZ and p-TTPAPZ before and after 100 cycles (Table S3)

12. Supplementary for detail description for behavior of charge storage (Table S4)

1.Material characterization

Chemical structure of the samples were proved by Fourier Transform Infrared spectrometer (FTIR) from Nicolet iS50 (Thermo Fisher, America) with KBr pellets in a test range of 4000 ~ 400 cm^{-1}. The microstructural morphology and distribution of the sample was observed by scanning electron microscope (SEM) using Regulus8100 (Hitachi, Japan). Thermogravimetric analyses (TGA) and differential thermal analysis (DTA) were performed on a thermogravimetric analyzer (Netzsch, Germany), running from room temperature to 800 ºC at a heating rate of 10 ºC. min^{-1} in N_2 atmosphere. X-ray photoelectron spectroscopy (XPS) was obtained on Axis Supra+ (Shimadzu, Japan). X-ray diffractometer (XRD) patterns were measured using D8 advance (BrukerGMBH, Germany), instrument operating at 40 kV and 40 mA and using Cu Kα radiation (λ = 0.15406 nm) with the scanning range from 5 to 70° and the scanning step at 0.02°. Brunner-Emmet-Teller (BET) measurement for the pore size distribution and specific surface area of the prepared materials was carried out on a Surface Area and Porosity Analyzer of ASAP2020 (McMurridge, USA), in which the samples were pretreated at 80 ºC under vacuum for 6 h with the N_2 as adsorbed gas.

2. Synthesis of 5,10-dihydrophenazine

The substance 5,10-dihydrophenazine was synthesized through a reduction reaction of phenazine (PZ) with sodium dithionite as reductant. A mixed solvent of ethanol (30 mL) and deionized water (120 mL) in a 250 mL round-bottom flask were firstly

degassed by sparging with nitrogen for 30 min. Phenazine (1.44 g, 8 mmol) and sodium dithionite (16.71 g, 96 mmol) were added above mixed solvent, which was refluxed and reacted under a nitrogen atmosphere until completely no solid blue particulate material remained. The reaction mixture was allowed to cool, quickly filtered, and the residue washed with deoxygenated water for three times to yield a light green powder. The product was dried and stored under vacuum until use.

3. FTIR description of p-DTPAPZ and p-TTPAPZ

Infrared spectroscopy (FTIR) analysis was performed for the resulted polymers of p-DTPAPZ and p-TTPAPZ. It can be seen that the infrared characteristic absorption peaks of the two polymers are basically similar, because of the similar chemical structures. It mainly includes the skeleton vibration peaks of the C-C and C=C bonds in the benzene ring at 1492.6cm^{-1} and 1596.8 cm^{-1}, the bending vibration peak of C-H in the benzene ring at 1324.8 cm^{-1}, the C-N stretching vibration peak from the tertiary amine at ~1268.9 cm^{-1} and the C-H out-of-plane vibration peak from the coexistence of 1,4-dissubstituted and mono-substituted benzene ring structure at ~823.4, 738.6 and 694.2 cm^{-1} in fingerprint region, respectively, which mainly occur in the benzene ring of the polymers. Above proves that two polytriphenylamine derivatives have been successfully synthesized by Buchwald-Hartwig cross-coupling polymerization. In addition, the specific intensity for the characteristic peaks of the mono-substituted benzene ring at around of 738.6 and 694.2 cm^{-1} becomes significantly stronger for p-DTPAPZ than that of p-TTPAPZ, indicating of the presence of more dangling mono-substituted benzene rings in the p-DTPAPZ.

4. Parameters obtained from the nitrogen desorption isotherm experiments (Table S1)

Table S1 Parameters obtained from the nitrogen desorption isotherm experiments

Sample	Specific surface area [m^2 g^{-1}]	Total pore volume [$cm^3 \cdot g^{-1}$]	Average aperture [nm]
p-DTPAPZ	110.916	0.532	12.861
p-TTPAPZ	25.782	0.083	41.416

5. TG and DTA analysis of p-DTPAPZ and p-TTPAPZ

The thermal stability for p-DTPAPZ and p-TTPAPZ samples was measured by the thermogravimetric analysis (TGA) and the differential thermal analysis (DTA) with the testing temperature range from room temperature to 800°C at a heating rate of 10 °C /min in the N_2 atmosphere (Figure S1), respectively. As shown, small weight loss before about 200°C for p-DTPAPZ and p-TTPAPZ is mainly corresponding to the loss of the physical adsorption water and the present small molecular. After the further temperature-programmed route, p-DTPAPZ and p-TTPAPZ shows a gradual thermogravimetric process, which corresponds to the gradual thermal degradation process of polymer skeleton. Comparatively, p-DTPAPZ polymer presents the relatively higher thermal stability than that of p-TTPAPZ. And there are ~78 wt% of the original material remained at the end of 800 ^oC for both materials. The differential thermal analysis (DTA) further indicates that p-DTPAPZ and p-TTPAPZ show the three exothermic peaks at 150-400°C, 400-600 °C and 600-800°C, respectively, which consistent to the results of thermogravimetric analysis.

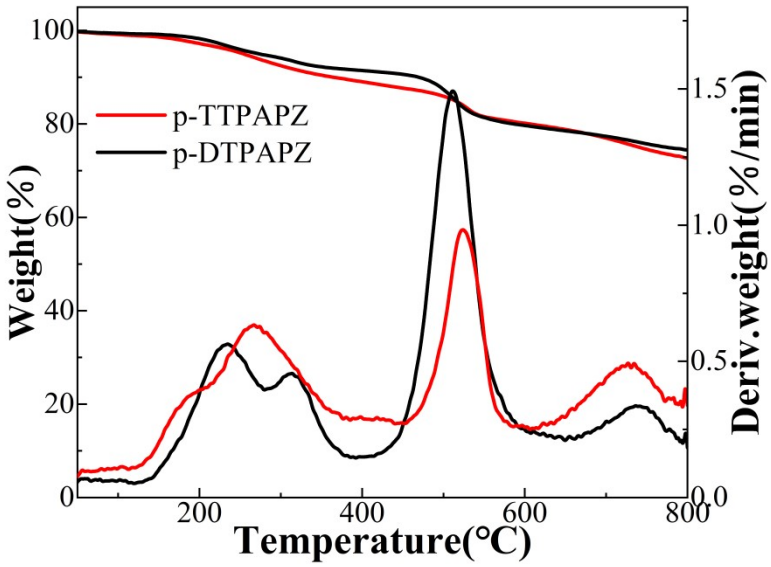

Figure S1 TG and DTA analysis of p-DTPAPZ and p-TTPAPZ.

6.Comparison of HOMO and LUMO energy orbitals of structure units of p-DTPAPZ and p-TTPAPZ in different electron-lose states.

To further confirm the multi-electron redox process and the potential change of p-DTPAPZ and p-TTPAPZ during the redox process, the density functional theory (DFT) calculation simulations were investigated. Since both p-DTPAPZ and p-TTPAPZ have the same repetitive structural units for redox process, the frontier molecular orbital analysis for the common molecular structural unit was performed, which contain the lowest unoccupied molecular orbital (LUMO) and the highest occupied molecular orbital (HOMO) energy levels of the repetitive structural units of p-DTPAPZ and p-TTPAPZ in different electron-lose states (Figure S2). As illustrated in Figure 8, the LUMO and HOMO energy levels locate at -0.99 and -4.36 eV for the repetitive structural units in the pristine state, at -4.28 and -7.69 eV for the repetitive structural units losing one electron, at -9.85 and-10.83 eV for the repetitive structural units losing two electrons, at -12.39 and-13.66 eV for the repetitive structural units

losing three electrons, respectively. It is widely acknowledged that HOMO energy level corresponds to the electronic ionization capability and oxidizing potential, while LUMO energy level is conversely consistent with the electron acceptability and reduction potential. For the repetitive structural units of p-DTPAPZ and p-TTPAPZ, the continuous decrease for the LUMO and HOMO energy levels indicates a gradual increase in the material's oxidation-reduction potential during the redox process, which companies with the muiti-electron losing process. And the result is consistent with the CV test results, indicating the multi-electron redox process for p-DTPAPZ and p-TTPAPZ. Accordingly, the narrower energy gap (E_g) between the HOMO and LUMO orbitals indicates the better conductivity of the material. For the repetitive structural units of p-DTPAPZ and p-TTPAPZ, the E_g values in different electron-lose states are 3.37, 3.41, 0.98 and 0.73 eV, in which E_g values decrease with losing electron, implying of the better charge migration stability and high electronic conductivity in the high redox state. It is obvious that the electron gain/loss process in electrode materials is accompanied by a significant change in electrode potential, which further confirms the multi-electron redox process of electrode materials in electrochemical processes.

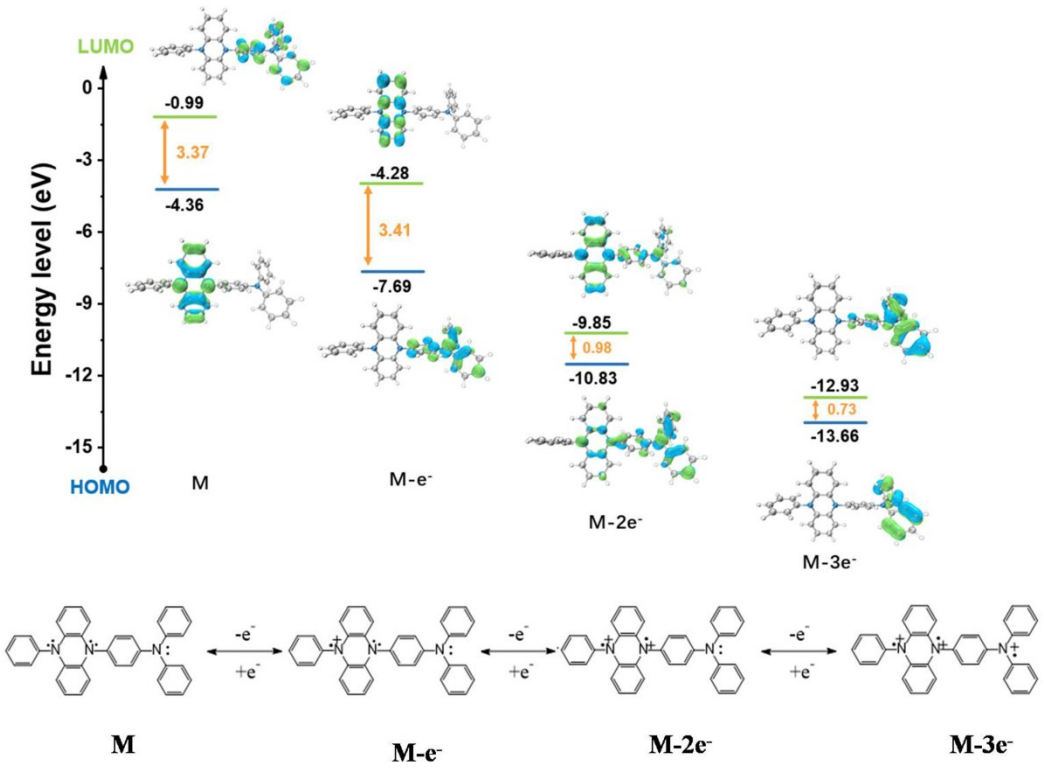

Figure S2 Comparison of HOMO and LUMO energy orbitals of structure units of p-DTPAPZ and p-TTPAPZ in different electron-lose states.

7.The electron spin resonance (ESR) analysis for p-DTPAPZ and p-TTPAPZ

The related analysis of the electron spin resonance (ESR) was performed, and the existence of a free radical in the products of p-DTPAPZ and p-TTPAPZ is confirmed by the electron spin resonance (ESR) (Figure S3), in which the nearly 2 of g values for p-DTPAPZ (2.0073) and p-TTPAPZ (2.00693) indicate the existence of the free radical in both polymers, respectively. To confirm that the two polymers are involved in a multi-electron redox reaction, the ESR of the polytriphenylamine (PTPA) polymer with a single electron redox characteristic was also measured using ESR. As a comparison of peak intensity, it can be seen that the two new polymers possess even more broad and strong peak intensities than the PTPA, indicative of the high free

radical density in the p-TTPAPZ and PTDATA, which implies that the multi-electron redox process will occur for the p-TTPAPZ and PTDATA as the cathode.

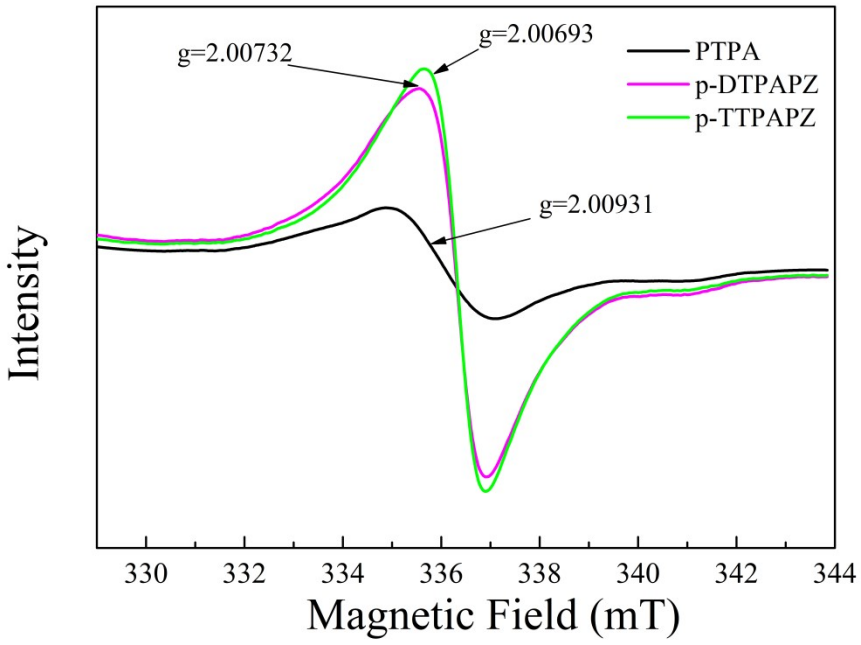

Figure S3 The electron spin resonance (ESR) for PTPA, p-DTPAPZ and p-TTPAPZ samples.

8. The charge-discharge curves and the corresponding differential capacity curves (dQ/dV) (c) (d) for p-DTPAPZ and p-TTPAPZ

In order to make the characteristic plateaus more clear, the charge and discharge curves for the p-DTPAPZ and p-TTPAPZ are redrawn as the form of the differential capacity curves (dQ/dV), in which p-DTPAPZ shows the two pairs of significant redox peaks and one pair of insignificant redox peaks at high potential, indicating the three redox process occurred during the discharge process. Comparatively, the p-TTPAPZ only exhibited two pairs of redox peaks. This indicates that the redox process for the triphenylamine unit is really occurred in the measured potential range.

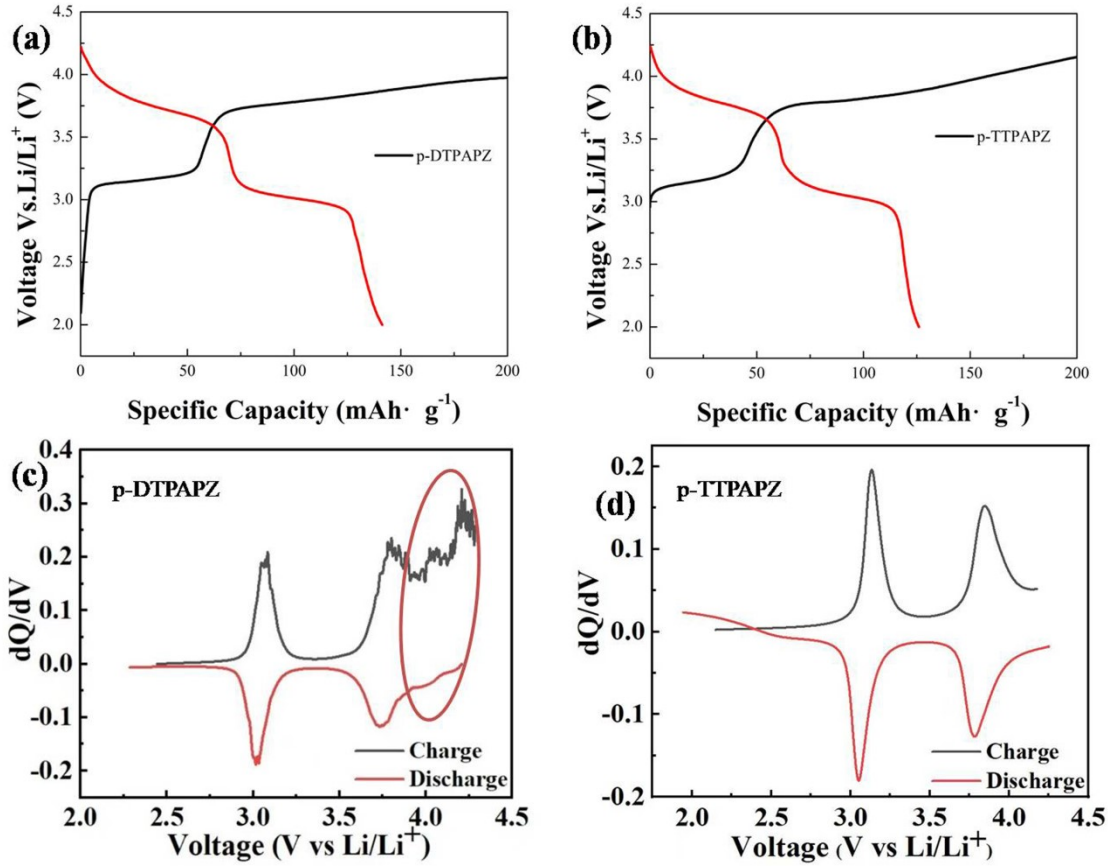

Figure S4 The charge-discharge curves (a) (b) and the corresponding differential capacity curves (dQ/dV) (c) (d) for p-DTPAPZ and p-TTPAPZ

9. Summary of the electrochemical performances for various arylamine based compounds and polymers as the cathode for Lithium ion batteries.

The added comparative table on the organic cathodes has been listed in the Table S2, in which our work presents a high reversible capacity and high rate performances. It indicates that preparing organic electrode materials with multi-electron redox characteristics through molecular design is a promising approach for the organic batteries with high performances.

Table S2 Summary of the electrochemical performances for various arylamine based compounds and polymers as the cathode for Lithium ion batteries.

Compound	Electrolyte	Average discharge voltage	Initial reversible capacity at current density	Rate capacity
PTPAn[28]	1M $LiPF_6$ in EC/DMC (v/v 1:1) electrolyte	~3.8 V	103 $mAh.g^{-1}$ at 54.5 $mA.g^{-1}$	90 $mAh.g^{-1}$ at 2180 $mA.g^{-1}$
PTDATA[30]	1M $LiPF_6$ in EC/DMC (v/v, 1 : 1) electrolyte	~3.5 V	133 $mAh.g^{-1}$ at 20 $mA.g^{-1}$	90.9 $mAh.g^{-1}$ at 500 $mA.g^{-1}$
PVK/MWNT[31]	1M $LiPF_6$ in EC/DMC (v/v, 1 : 1) electrolyte	~2.0 V	115 $mAh.g^{-1}$ at 20 $mA.g^{-1}$	/
PVMPT[33]	1M $LiPF_6$ in EC/DMC (v/v, 1 : 1) electrolyte	~3.5 V	112 $mAh.g^{-1}$ at 20 $mA.g^{-1}$	85 $mAh.g^{-1}$ at 10 C
PVMPO[34]	1M $LiPF_6$ in EC/DMC (v/v, 1 : 1) electrolyte	~3.52 V	112 $mAh.g^{-1}$ at 0.5 C	~68 $mAh.g^{-1}$ at 100 C
p-DPPZS[36]	1M $LiPF_6$ in EC/DEC (v/v, 1 : 1) electrolyte	~3.48 V	133 $mAh.g^{-1}$ at 0.5 C	64 $mAh.g^{-1}$ at 20 C
PZDB[37]	1M $LiPF_6$ in EC/DEC (v/v, 1 : 1) electrolyte	~2.75 V	57 $mAh.g^{-1}$ at 1 C	45 $mAh.g^{-1}$ at 2 C
DMPZ[38]	0.1 M LiTFSI in TEGDME	~3.31 V	191 $mAh.g^{-1}$ at 50 $mA.g^{-1}$	/
p-DPPZ[41]	1M $LiPF_6$ in EC/DEC (v/v, 1 : 1) electrolyte	~3.5 V	150 $mAh.g^{-1}$ at 0.5 C	65 $mAh.g^{-1}$ at 5 C
This work	1M $LiPF_6$ in EC/DMC (v/v, 1 : 1) electrolyte	~3.45 V	160.1 $mAh.g^{-1}$ at 30 $mA.g^{-1}$	94.4 $mAh.g^{-1}$ at 1000 $mA.g^{-1}$

10. The electrochemical impedance test (EIS) of p-DTPAPZ and p-TTPAPZ samples

The electrochemical impedance test (EIS) of p-DTPAPZ and p-TTPAPZ before and after 100 cycles was performed in the frequency range of 0.01 Hz-100kHz. As can be seen from Figure S5a and S5b, the Nyquist spectra are mainly composed of two parts: the semi-circular at high frequency region for the electron transfer resistance at the electrode/electrolyte interface and a linear at low frequency region corresponding to the Warburg impedance related to lithium ion diffusion respectively. Based on the measured spectra, the equivalent circuit was fitting by software, and the simulation results are listed in Table S3, which include battery resistance (ESR), charge-transfer reaction resistance (R_{cr}), double layer capacitance and passivation film capacitance (CPE) and Warburg Impedance (W_r). For samples before 100 cycles, the data of ESR, R_{cr}, CPE and W_r are 2.8 Ω, 176.1 Ω, 3.97×10^{-5} μF, 297.1 Ω for p-DTPAPZ and 2.9 Ω, 315.4 Ω, 3.83×10^{-5} μF, 514.2 Ω for p-TTPAPZ, respectively, in which the smaller R_{cr} and W_r demonstrate more proficient charge transfer and ion penetration for p-DTPAPZ electrode. This is mostly due to the constructed aromatic amine conjugated molecular skeleton structure and a porous loose morphology, which promotes rapid electron transfer and ion diffusion among electrode-electrolyte interface, leading to low charge transfer resistance. Comparatively, the values of ESR, R_{cr}, CPE and W_r for p-DTPAPZ increase a litter after 100 cycles, suggesting the stable structure and reaction kinetics.

For the detailed investigation, impedance behavior for p-DTPAPZ and p-TTPAPZ

samples were further indicated by Bode absolute and Bode phase diagrams. As shown in Figure S5c and S5d, p-DTPAPZ exhibits smaller impedance value (Z) than p-TTPAPZ at the lower Frequency, which is consistent with Nyquist result. Based on the Bode angle diagram, it is observed that the intersect values in the low-frequency region for p-DTPAPZ and p-TTPAPZ electrodes lies between 40^{o} and 80^{o}, which is the characteristic capacitance or adsorption behavior of electrode materials. While the intersect values in the high-frequency region tend to zero, implying of resistive nature.

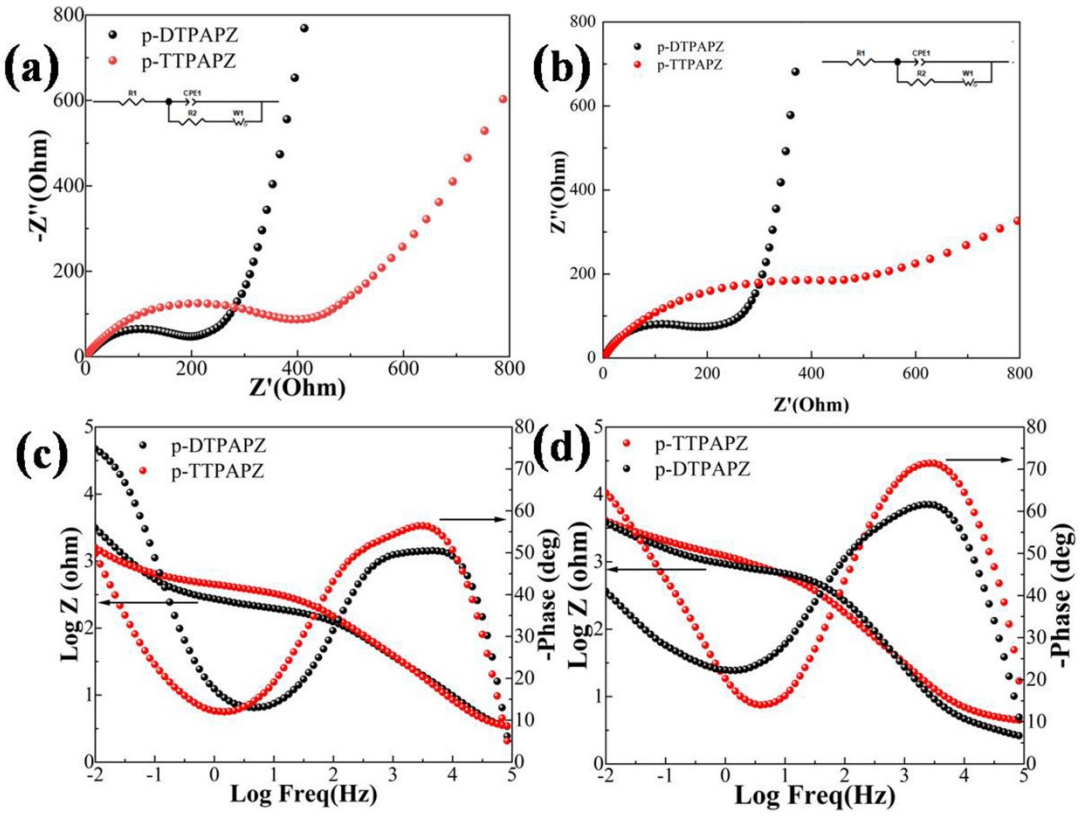

Figure S5 Nyquist spectra of p-DTPAPZ (a) and p-TTPAPZ (b) samples in Li/electrolyte/sample configuration before and after the cycling. Insert: Equivalent circuit; Bode plot of polymers p-DTPAPZ (c) and p-TTPAPZ (d) samples.

11. Equivalent circuit data of p-DTPAPZ and p-TTPAPZ before and after 100 cycles

Table S3 Equivalent circuit data of p-DTPAPZ and p-TTPAPZ before and after 100 cycles

Sample	R_{cell}(Ω)	R_s(Ω)	R_{ct}(Ω)	W_r(Ω)	CPE（μF）
p-DTPAPZ (before)	201	2.8	176.1	297.1	3.97×10^{-5}
p-TTPAPZ (after)	410	2.9	315.4	514.2	3.83×10^{-5}
p-DTPAPZ (before)	231	3.1	188.6	323.1	8.01×10^{-6}
p-TTPAPZ (after)	464	4.0	354.5	562.3	9.34×10^{-6}

12. Detail description for behavior of charge storage

Usually, electrode material storage is mainly divided into two mechanical processes: the capacitance process and the diffusion control Faraday process. Electrochemical analysis was further carried out in the test voltage range of 2.0-4.5 V to explore the behavior of charge storage for p-DTPAPZ and p-TTPAPZ electrode materials. For the two electrode materials, the cyclic voltammetry (CV) was further measured at different scan speeds of 1, 2, 3, 5, 7, and 10 $mV\cdot s^{-1}$, respectively. As shown in the Figure 6a and 6b, it can be observed that with the increase of sweep speed, the peak current gradually increases, indicating that the electrochemical activity is gradually enhanced, but the shape of the pattern does not change much, indicating that the polymer itself is less polarized at high sweep speed, and the electrochemical properties of the substance are stable. Normally, the energy storage process and capacitive effect can be expressed by the classic formula: $i=av^b$ or $log\ i = b log\ v + log\ a$, where *i*-peak current, *v*-peak current corresponding sweep rate, *a*-and *b*-variable

parameters. Theoretically, *b* value close to 0.5 indicates that the electrochemical process is mainly controlled by diffusion behavior (faradaic), while a value of *b* close to 1.0 indicates that the reaction process is mainly controlled by capacitive behavior (nonfaradaic). Figure 5c shows the log(*i*) *vs*. log(*v*) plot for p-DTPAPZ and p-TTPAPZ, from which the calculated *b* values were 0.72, 0.64, 0.78 and 0.85 for the peaks A1, A2, A3 and A4 of p-TTPAPZ and 0.72, 0.71, 0.83, 0.87, 0.97 and 0.94 for the peaks A1, A2, A3, A4, A5 and A6 of p-DTPAPZ, respectively. All of the values of *b* were in the range of 0.5 to 1, suggesting that the storage mechanism of lithium is mainly controlled by the surface capacitance-diffusion hybrid control kinetics. Also, p-DTPAPZ has a large *b* value than that of p-TTPAPZ, implying that the p-DTPAPZ electrode material has more the energy storage contribution from surface capacitance process than that of p-TTPAPZ.

Based on Randles-Sevcik equation, $i_p = (2.69\times10^5)\cdot n^{3/2}\cdot A\cdot D_{Li+}^{1/2}\cdot C_{Li}\cdot v^{1/2}$, where n, A and $C_{Li,}$is the charge-transfer number, geometric area of electrode (cm^2) and concentration of lithium ions in the cathode ($mol\cdot cm^3$), respectively, the apparent diffusion coefficient values were calculated from the slope of i_p vs. $v^{1/2}$ plots in Figure 6d, and the results were shown in Table S4. Obviously, p-DTPAPZ has relatively smaller the values than p-TTPAPZ, indicative of the faster interface charge transfer for p-DTPAPZ, which is consistent with higher surface capacitance process of p-DTPAPZ.

Table S4 Diffusion coefficients at the anode and cathode scanning for p-DTPAPZ and p-TTPAPZ.

Sample	Diffusion Coefficient ($cm^2 \cdot s^{-1}$)					
p-DTPAPZ	A1	A2	A3	A4	A5	A6
	1.78×10^{-10}	7.11×10^{-11}	2.25×10^{-10}	1.92×10^{-10}	1.98×10^{-10}	8.80×10^{-11}
p-TTPAPZ	B1	B2	B3	B4		
	1.82×10^{-11}	1.76×10^{-11}	3.42×10^{-11}	2.49×10^{-11}		

The total capacity contributed from capacitive and diffusive process for electrode materialis can been also expressed by $C=\int i dV/(7.2vm)$, where C is the specific capacity ($mAh \cdot g^{-1}$),v is the potential scan rate ($V \cdot s^{-1}$), m is the active mass loading (g), and i is the voltammetric current (A). Therein, the voltammetric current (A) (i) can be distinguished as pseudocapacitive current (a_1v) and diffusion-controlled faradaic current ($a_2v^{0.5}$) at a given scan rate, according to the total current formula of $i = a_1v + a_2v^{1/2}$. As depicted in Figure 7, p-DTPAPZ exhibits a higher capacitive contribution of 90 % than that of p-TTPAPZ (79 %) at 1.0 mV s^{-1}, which can be attributed to the developed porous fiber morphology of p-DTPAPZ and the resulting large number of reactive sites undergoing redox reactions. In addition, the contribution ratios from capacitive process increase with the increase of scanning rates from 1.0 mV s^{-1} to 10 mV s^{-1}. Obviously, the higher the scan rates are, the greater the proportion of capacitive behavior, indicating that p-DTPAPZ has a fast kinetic process and excellent rate performance.